Cholesterol loss during glutamate-mediated excitotoxicity

Alejandro O Sodero[1], Joris Vriens[2],
Debapriya Ghosh[2], David Stegner[3],
Anna Brachet[4], Marta Pallotto[5],
Marco Sassoè-Pognetto[5], Jos F Brouwers[6],
J Bernd Helms[6], Bernhard Nieswandt[3],
Thomas Voets[2] and Carlos G Dotti[1,4]*

[1]VIB Center for Biology of Disease, Katholieke Universiteit Leuven, Leuven, Belgium, [2]Department of Molecular Cell Biology, Laboratory of Ion Channel Research, Katholieke Universiteit Leuven, Leuven, Belgium, [3]Rudolf Virchow Center for Experimental Biomedicine and Chair of Vascular Medicine, University Hospital, University of Würzburg, Würzburg, Germany, [4]Centro de Biología Molecular Severo Ochoa, CSIC-UAM, Madrid, Spain, [5]Department of Anatomy, Pharmacology and Forensic Medicine, University of Turin and National Institute of Neuroscience, Torino, Italy and [6]Department of Biochemistry and Cell Biology, Faculty of Veterinary Medicine, Utrecht University, Utrecht, The Netherlands

The deregulation of brain cholesterol metabolism is typical in acute neuronal injury (such as stroke, brain trauma and epileptic seizures) and chronic neurodegenerative diseases (Alzheimer's disease). Since both conditions are characterized by excessive stimulation of glutamate receptors, we have here investigated to which extent excitatory neurotransmission plays a role in brain cholesterol homeostasis. We show that a short (30 min) stimulation of glutamatergic neurotransmission induces a small but significant loss of membrane cholesterol, which is paralleled by release to the extracellular milieu of the metabolite 24S-hydroxycholesterol. Consistent with a cause–effect relationship, knockdown of the enzyme cholesterol 24-hydroxylase (CYP46A1) prevented glutamate-mediated cholesterol loss. Functionally, the loss of cholesterol modulates the magnitude of the depolarization-evoked calcium response. Mechanistically, glutamate-induced cholesterol loss requires high levels of intracellular Ca^{2+}, a functional stromal interaction molecule 2 (STIM2) and mobilization of CYP46A1 towards the plasma membrane. This study underscores the key role of excitatory neurotransmission in the control of membrane lipid composition, and consequently in neuronal membrane organization and function.

*Corresponding author. Centro de Biología Molecular Severo Ochoa, CSIC/UAM. Nicolás Cabrera 1, Campus de la Universidad Autónoma de Madrid, 28049 Madrid, Spain. Tel.: +34 911964534;
Fax: +34 911964420; E-mail: cdotti@cbm.uam.es

Introduction

Cholesterol is essential for the normal functioning of most eukaryotic cells. As a major component of the plasma membrane (PM), cholesterol plays a key role in fluidity and permeability and, together with sphingolipids, constitutes membrane microdomains or rafts (Lingwood and Simons, 2010). Rafts are known to regulate a panoply of functions, including endocytosis and intracellular signalling for differentiation and cell survival (Simons and Toomre, 2000; Tsui-Pierchala *et al*, 2002). Given such functional pleiotropism, it is evident that cholesterol is a major regulator of neuronal function. Consistently, a series of recent reports have demonstrated the importance of cholesterol in the control of synaptic transmission. Acute cyclodextrin-mediated removal of membrane cholesterol inhibits synaptic transmission and plasticity in the hippocampus (Frank *et al*, 2008), whereas a reduction in cholesterol synthesis enhances hippocampal long-term potentiation (Mans *et al*, 2010). Cholesterol reduction also affects the viscosity of the post-synaptic density (Renner *et al*, 2009) and impairs proton and glutamate storage in synaptic vesicles (Tarasenko *et al*, 2010). In addition, it has recently been shown that cholesterol synthesis and catabolism are differentially affected at distinct times in models of glutamate-mediated excitotoxicity (Ong *et al*, 2010). From these findings, it seems reasonable to hypothesize that at least some of the typical signs and symptoms of the pathological conditions that are accompanied by excessive glutamatergic neurotransmission, such as stroke, epileptic seizures or traumatic brain injury, may be due to glutamate-triggered cholesterol dyshomeostasis.

The major rate-limiting enzyme in the cholesterol synthesis pathway is the endoplasmic reticulum (ER)-bound 3-hydroxy-3-methylglutaryl-coenzyme-A reductase, which produces mevalonate. After this step, cholesterol synthesis follows two alternative routes: one route leads to production of desmosterol as an immediate precursor of cholesterol; the other leads to production of 7-dehydrocholesterol as a direct precursor. Next, 7-dehydrocholesterol is converted to cholesterol by the enzyme 7-dehydrocholesterol Δ7-reductase. It has been proposed that in the adult stage, when membrane addition has largely stopped, neurons rely on astrocytes for the energy intensive process of cholesterol synthesis. Evidence for a cholesterol shuttle from astrocytes to neurons has been presented (Michikawa *et al*, 2000; Gong *et al*, 2002), and it has also been demonstrated *in vitro* that neurons require cholesterol delivery from glial cells to form synapses (Göritz *et al*, 2002). In further support of the theory that neurons delegate this costly metabolic pathway to astrocytes, mature neurons have been shown to produce cholesterol inefficiently and to have a much lower capacity to upregulate the cholesterol synthetic pathway than astrocytes (Nieweg *et al*, 2009).

A small fraction of brain cholesterol (∼0.02% in humans and ∼0.4% in mice) turns over each day (Dietschy and

Turley, 2004). The major mechanism of cholesterol removal is its conversion into 24S-hydroxycholesterol, which diffuses out of the neurons, crosses the blood–brain barrier and is cleared by the liver (Lütjohann, 2006). This reaction is catalysed by a cytochrome P450 enzyme, cholesterol 24-hydroxylase (CYP46A1), which is selectively expressed in the brain (Lund *et al*, 1999). High levels of this enzyme are found in neuronal cells, specifically in the pyramidal neurons of the hippocampus and cortex, in the Purkinje cells of the cerebellum, and in hippocampal and cerebellar interneurons (Ramirez *et al*, 2008).

In the present study, we show that hippocampal neurons that exhibit high levels of excitatory, but not inhibitory, neurotransmission experience a mild loss of membrane cholesterol through a Ca^{2+}/STIM2-mediated mobilization of CYP46A1 from the smooth ER towards the PM.

Results

Excitatory neurotransmission induces hippocampal membrane cholesterol loss in vitro and in vivo

Neurotransmitters are released from axon terminals by vesicular exocytosis. Exposure of neurons to elevated concentrations of KCl is a conventional procedure to elicit this neurotransmitter release (Jahn and Südhof, 1994). Therefore, to test whether glutamate receptor activation plays a role in the regulation of membrane cholesterol, 14-day *in-vitro* rat hippocampal neurons were incubated for 30 min with 55 mM KCl, and the effect of this incubation on cholesterol levels was evaluated in the membrane extracts at the end of the incubation period. High levels of potassium induced a significant reduction in the content of membrane cholesterol ($21.5 \pm 2.4\%$, Figure 1A).

We have previously demonstrated that 55 mM KCl mediates dendritic spine plasticity via a glutamate-mediated effect in cultured hippocampal neurons (Schubert *et al*, 2006), suggesting that KCl effects might be preponderantly postsynaptic. However, since KCl-induced glutamate release can lead to global depolarization, action potential firing and secondary activation of voltage-gated channels, we tested if KCl-mediated cholesterol loss could still occur in the presence of the sodium channel blocker tetrodotoxin (TTX). Also under this condition, 55 mM KCl effectively induced cholesterol loss (Supplementary Figure S1). To further validate the postsynaptic nature of this effect, cultured hippocampal neurons were challenged for 30 min with 1, 10 and 100 μM of the glutamate receptor agonist N-methyl-D-aspartate (NMDA). Treatment with this agonist produced a reduction in the membrane cholesterol levels, which was significant even for 10 μM NMDA ($18.6 \pm 3.3\%$, Figure 1A). With a concentration of 100 μM NMDA, the decrease in cholesterol levels was slightly higher ($26.7 \pm 7.3\%$, Figure 1A). Although the applied concentrations of NMDA increase neuronal death after 24 h, some consequences after 30 min, like in our experiments, could be beneficial for the cell (Papadia and Hardingham, 2007; Papadia *et al*, 2008; Léveillé *et al*, 2010). In agreement, neuronal morphology, viability and expression of synaptic proteins were not affected by exposure to NMDA for 30 min (Supplementary Figure S2).

To validate the specificity of the NMDA-induced effect, cultured neurons were exposed to 10 μM NMDA in the presence of 10 μM of the specific NMDA receptor antagonist
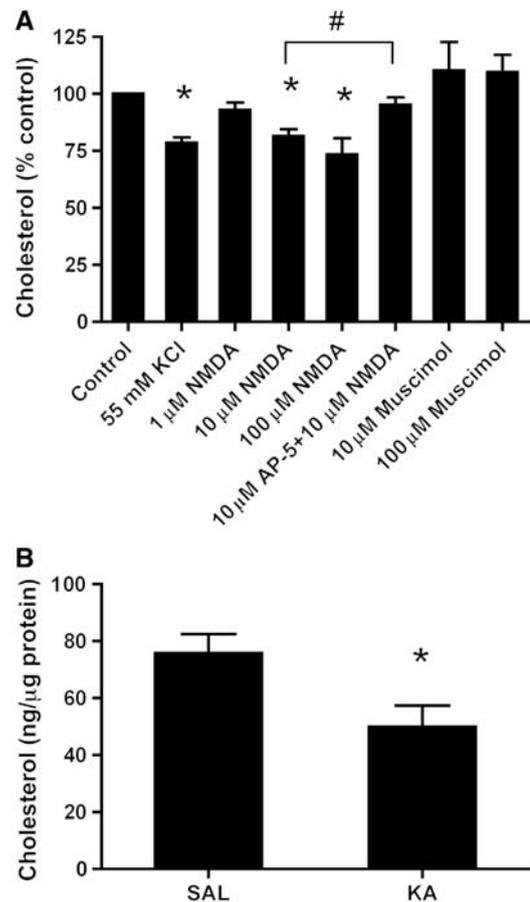

Figure 1 Excitatory neurotransmission induces hippocampal membrane cholesterol loss. (**A**) Induction of glutamate release with 55 mM KCl or direct stimulation of postsynaptic NMDA receptors with 10 or 100 μM NMDA, but not 1 μM NMDA, induces a significant cholesterol loss in the membranes of cultured hippocampal neurons. Preincubation with the NMDA receptor antagonist DL-2-Amino-5-phosphonopentanoic acid (AP-5, 10 μM) for 10 min rescued the cholesterol loss that was induced by 10 μM NMDA. Strengthening of inhibitory neurotransmission by the addition of 10 or 100 μM muscimol did not significantly affect the cholesterol levels. In all the cases, the treatments were performed for 30 min. The cholesterol levels were assessed using fluorimetric detection, normalized to the amount of protein and expressed as a percentage of change relative to the corresponding control. The protein levels did not differ significantly between the treated hippocampal neurons and their controls after 30 min of treatment. In this and all of the subsequent figures, the bars represent the mean and the error bars represent the s.e.m. ($n = 4$–7, $*P < 0.05$ versus control, $\#P < 0.02$, Student's *t*-test). (**B**) Mice were injected with kainic acid (KA, 20 mg/kg i.p.) to stimulate excitatory neurotransmission. The corresponding controls were injected with a saline solution. Hippocampal membranes were purified 30 min later, and the cholesterol levels were assessed using fluorimetric detection. KA treatment induced a significant cholesterol reduction in the hippocampal membranes (SAL: 75.8 ± 6.7 versus KA: 50.0 ± 7.4 ng cholesterol/μg protein; $n = 4$, $*P < 0.05$ versus SAL, Student's *t*-test).

DL-2-Amino-5-phosphonopentanoic acid (AP-5). This manipulation prevented the NMDA-induced cholesterol loss (Figure 1A).

To test whether cholesterol loss also occurs during increased inhibitory transmission, cultured hippocampal neurons were incubated for 30 min with 10 and 100 μM of the GABA$_A$ receptor agonist muscimol. In contrast to the NMDA receptor activation, activation of inhibitory GABA$_A$ receptors did not produce significant changes in cholesterol levels after 10 or 100 μM muscimol (Figure 1A).

To investigate whether increased excitatory neurotransmission leads to cholesterol loss *in vivo*, we measured the amount of this lipid in hippocampal membranes that were purified from mice 30 min after a single injection (20 mg/kg, i.p.) of kainic acid (KA). At this time point, KA causes an activation of CA3 pyramidal neurons and CA3 recurrent synapses (Ben-Ari and Cossart, 2000). Similarly to the *in-vitro* condition, the hippocampal membranes that were obtained from the KA-treated mice exhibited an average reduction of 34.0% in the amount of cholesterol compared with those of the saline-treated mice (Figure 1B). In further agreement, liquid chromatography/mass spectrometry (LC/MS) analysis of whole hippocampal tissue showed a significant reduction in the cholesterol/phospholipids ratio in KA-treated animals compared with saline-treated animals (SAL: 0.57 ± 0.01 versus KA: 0.53 ± 0.01; $P < 0.05$, Student's t-test).

Glutamate-mediated cholesterol loss is synaptic

While the experiments with the specific NMDA receptor antagonist AP-5 confirmed the synaptic nature of the glutamate-mediated cholesterol loss, we further analysed this event using purified synaptosomes. First, we exposed synaptosomes to 55 mM KCl and analysed their cholesterol content 15 min later. This treatment resulted in a significant loss of cholesterol ($19.9 \pm 2.7\%$, Figure 2A). Next, we measured the cholesterol content in synaptosomes that were incubated with 10 μM NMDA (30 min) or 10 μM AMPA (15 min). These treatments also resulted in a significant reduction in synaptic cholesterol (10.7 ± 2.6 and $13.3 \pm 4.9\%$, respectively; Figure 2A). The combination of 10 μM NMDA and 10 μM AMPA for 30 min led to a larger reduction in cholesterol ($20.2 \pm 3.3\%$, Figure 2A). In contrast, the addition of 50 μM muscimol did not alter the cholesterol levels (Figure 2A). Consistent with the results from the whole hippocampal membrane fractions, the isolated synapses of KA-treated mice exhibited an average cholesterol reduction of 31.7%, 30 min after the injection (Figure 2B). Hence, cholesterol loss appears to be a natural response to excessive excitatory neurotransmission, even in purified synapses. Since the largest pool of cholesterol is at the PM, and mitochondria and SER tubules, which are also present in the synaptosomal fractions, contain just 0.1–2% of the total cellular cholesterol (Lange, 1991; Pomorski *et al* 2001; Lebiedzinska *et al*, 2009), we find it reasonable to conclude that the majority of the observed cholesterol loss in our experimental conditions occurs at the PM.

NMDA-mediated cholesterol loss plays a role in the modulation of the intracellular calcium response

To determine the functional relevance of the NMDA-mediated cholesterol loss, intracellular Ca^{2+} levels were monitored in neurons exposed to depolarizing stimuli. Under control conditions, two depolarizing stimuli (high K^+) applied with an interval of 30 min evoked calcium transients of comparable amplitude (Figure 3A). However, when in between the two stimuli the cells were exposed to 10 μM NMDA the response to the second stimulus was significantly reduced (Figure 3B). In agreement with the possibility that this effect was due to NMDA-mediated cholesterol loss, delivery of small amounts of cholesterol (see Materials and methods) in between the two stimuli prevented the reduction in the second Ca^{2+} response produced by 10 μM NMDA (Figure 3B). In further
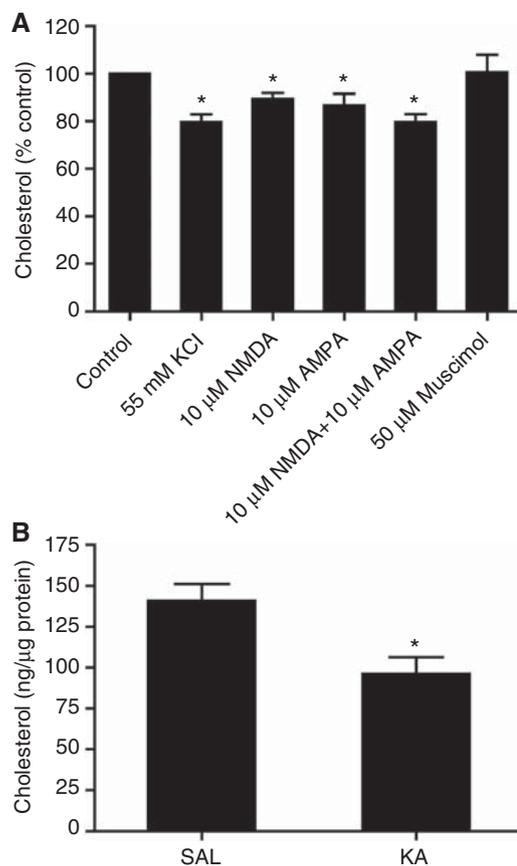

Figure 2 Cholesterol loss induced by excitatory neurotransmission is synaptic. (**A**) Stimulation of rat brain synaptosomes with 55 mM KCl (15 min) induces cholesterol loss from the synaptic membranes. Stimulation of ionotropic receptors that are associated with Ca^{2+} influx by incubation with 10 μM NMDA (30 min), 10 μM AMPA (15 min) or a combination of 10 μM NMDA and 10 μM AMPA (30 min) induces a significant cholesterol loss. Incubation with 50 μM muscimol (15 min), a GABA$_A$ receptor agonist that increases Cl^- influx, does not change synaptic cholesterol content ($n = 4$–9, $^*P < 0.05$ versus control, Student's t-test). (**B**) Mice were injected with kainic acid (KA, 20 mg/kg i.p.) to promote excitatory neurotransmission. The corresponding controls were injected with a saline solution. Synaptic membranes were purified 30 min later, and the cholesterol levels were assessed using fluorimetric detection. KA treatment induced a significant cholesterol loss (SAL: 140.8 ± 10.2 versus KA: 96.2 ± 10.0 ng cholesterol/μg protein; $n = 4$, $^*P < 0.03$ versus SAL, Student's t-test).

agreement, treatment of neurons with 0.1 mM methyl-β-cyclodextrin (MBCD), which binds and removes cholesterol from the PM (Rodal *et al*, 1999), induced a reduced Ca^{2+} response to the second stimulus (Figure 3A) Taken together, these data indicate that NMDA leads to reduced depolarization-evoked Ca^{2+} response, which is, at least partly, due to NMDA-induced cholesterol loss.

Glutamate-mediated cholesterol loss requires high levels of intracellular calcium

To test whether cholesterol loss under depolarizing conditions requires a high level of intracellular Ca^2, synaptosomes were incubated with 55 mM KCl, which activates voltage-gated Ca^{2+} channels, and cholesterol levels were assessed after 15 min. When the synaptosomes were incubated in Ca^{2+}-containing physiological buffer, the 55 mM KCl
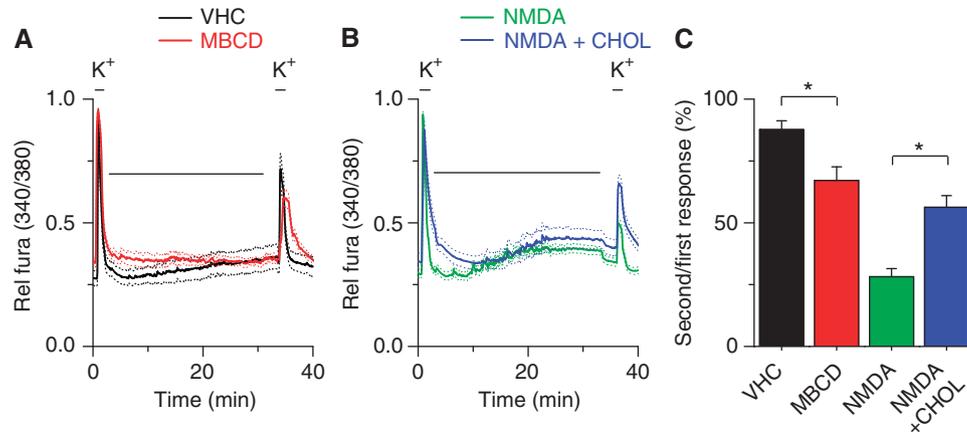
Figure 3 Modulation of intracellular calcium levels by NMDA-induced cholesterol loss. (**A**) Time course of the ratiometric calcium signal in 14 *div* hippocampal neurons, showing the response to two pulses with 50 mM KCl, applied with an interval of 30 min. During this interval, neurons were exposed to Krebs solution (VHC, black) or 0.1 mM methyl-β-cyclodextrin (MBCD, red). (**B**) Time course of the ratiometric calcium signal in response to two pulses with 50 mM KCl. During the 30-min interval, neurons were exposed to 10 μM NMDA (NMDA, green) or to 10 μM NMDA in the presence of 30 μM water-soluble cholesterol/5.2 μM cholesterol (NMDA + CHOL, blue). (**C**) Statistical analysis of the ratio between the second and the first response to 50 mM KCl (*$P < 0.01$, Student's t-test).
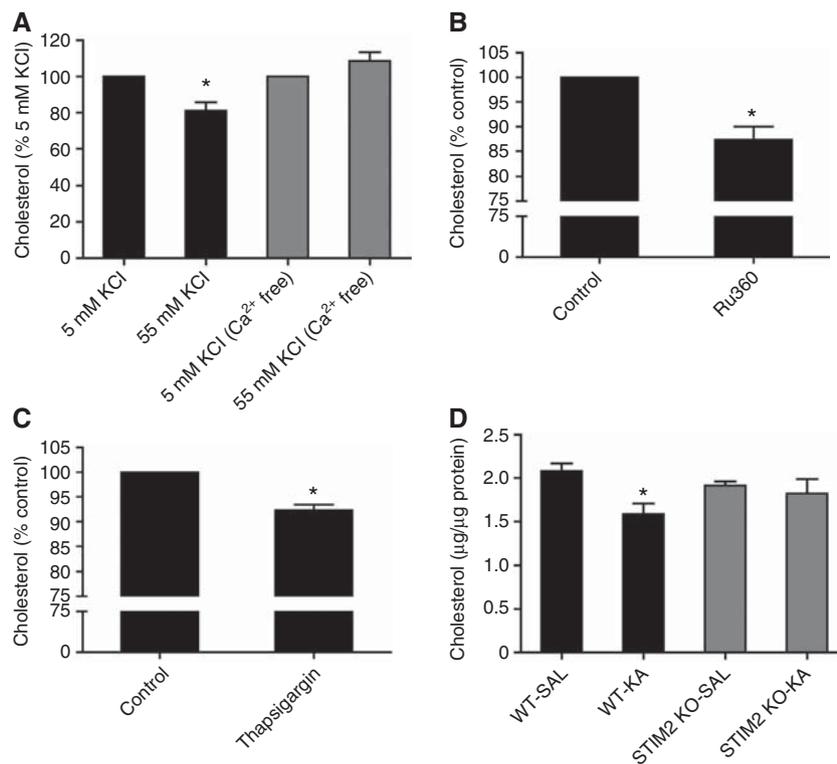

Figure 4 Synaptic cholesterol loss depends on intracellular Ca^{2+} rise and requires a functional STIM2. (**A**) Rat brain synaptosomes were incubated with 55 mM KCl in normal buffer or in Ca^{2+}-free buffer/1 mM EGTA, and the cholesterol levels were assessed 15 min later ($n = 3$; *$P < 0.05$ versus 5 mM KCl, Student's t-test.). (**B**) Incubation of synaptosomes for 30 min with 10 μM Ru360 to raise intracellular Ca^{2+} levels by inhibition of the mitochondrial Ca^{2+} uptake ($n = 3$; *$P < 0.05$ versus control, Student's t-test). (**C**) Incubation of synaptosomes for 10 min with 10 μM thapsigargin in Ca^{2+}-free buffer/1 mM EGTA to produce ER Ca^{2+} depletion ($n = 4$; *$P < 0.05$ versus control, Student's t-test). (**D**) Wild-type (WT) and STIM2 knockout (KO) mice were injected with saline (SAL) or 20 mg/kg i.p. kainic acid (KA). After 30 min, brain synaptosomes were purified and membrane cholesterol was assessed ($n = 6$ for WT, $n = 4$ for KO; *$P < 0.01$ versus WT-SAL, Student's t-test).

triggered cholesterol loss; however, this was not the case when the synaptosomes were exposed to 55 mM KCl in a Ca^{2+}-free buffer (Figure 4A). To further demonstrate the role of intracellular Ca^{2+}, synaptosomes were exposed to 10 μM Ru360, a selective blocker of the mitochondrial Ca^{2+} uniporter

that increases the cytoplasmic Ca^{2+} concentration independently of PM channels (Nicholls and Chalmers, 2004). This treatment also triggered significant synaptic cholesterol loss after 30 min ($12.7 \pm 2.7\%$, Figure 4B), altogether suggesting that intracellular Ca^{2+} raise is necessary and sufficient for

cholesterol loss. However, by no means the observed effects with Ru360 imply the involvement of mitochondrial calcium in glutamate-induced cholesterol loss. In fact, it has been demonstrated that the intracellular Ca^{2+} signal that follows the activation of ionotropic glutamate receptors can be amplified by Ca^{2+} release from the ER (Ruiz *et al*, 2009). To test if releasing Ca^{2+} from intracellular stores also produces cholesterol loss, synaptosomes were incubated in Ca^{2+}-free buffer with 10 µM thapsigargin, which leads to ER depletion by virtue of its non-competitive inhibition of SERCA (sarco/ER Ca^{2+} ATPase) (Rogers *et al*, 1995). In agreement with the prediction, thapsigargin induced a significant loss of cholesterol ($7.7 \pm 1.1\%$, Figure 4C). Then, we hypothesized that glutamate-induced cholesterol loss may be modulated by STIM2, an ER Ca^{2+}-sensing molecule that has been shown to be essential for store-dependent Ca^{2+} signalling in neurons (Berna-Erro *et al*, 2009). Interestingly, we found that a single injection of KA (20 mg/kg, i.p.) caused a significant cholesterol decrease in the synapses of WT mice, and this effect was strongly reduced in the STIM2 knockout mice (Figure 4D). Taken together, these data indicate that glutamate-mediated cholesterol loss involves ER-dependent Ca^{2+} signalling.

Excitatory neurotransmission and high levels of intracellular Ca^{2+} mobilize CYP46A1 towards the PM

A major route for the removal of cholesterol from the brain is thought to be the enzymatic conversion of cholesterol into 24S-hydroxycholesterol by the enzyme CYP46A1 (Lund *et al*, 1999; Björkhem and Meaney, 2004). In agreement, the cholesterol loss triggered by the addition of NMDA to hippocampal neurons in culture was paralleled by a significant increase in the levels of 24S-hydroxycholesterol in the medium. Consistently with a direct cause–effect relationship, knockdown of CYP46A1 prevented glutamate-mediated cholesterol loss in cultured neurons (Supplementary Figure S3). Recent data have confirmed the exclusive neuronal expression of this enzyme and its preferential localization in the ER of dendrites and cell bodies (Ramirez *et al*, 2008). Hence, one possibility to explain the observed cholesterol loss is the mobilization of CYP46A1 from the ER to the PM. Consistent with this hypothesis, studies in hepatocytes have demonstrated that another member of the Cytochrome P450 family reaches the PM from the ER via a vesicular pathway (Robin *et al*, 2000). Our electron microscopy studies show that CYP46A1 is present both in intracellular membranes and in the PM of hippocampal synapses (Figure 5), suggesting the existence of a similar ER to the PM pathway. In addition, electron microscopy quantifications of hippocampal dendritic profiles in KA-injected mice showed a significant increase in the amount of CYP46A1 associated with the PM compartment (saline injected: 83/466 PM/total gold particles, 17.8% versus KA injected: 88/340 PM/total gold particles, 25.9%; $P < 0.01$, Fisher's exact test). To address this possibility more directly, we performed surface biotinylation experiments in cultured hippocampal neurons that were exposed to 55 mM KCl, using a membrane-impermeable biotin. These experiments revealed a mild but significant increase in the amount of surface CYP46A1 ($16.0 \pm 5.1\%$, Figure 6), without changes in the expression levels of this enzyme.

To more conclusively test the mobilization towards the PM, we used Total Internal Reflection Fluorescence (TIRF)
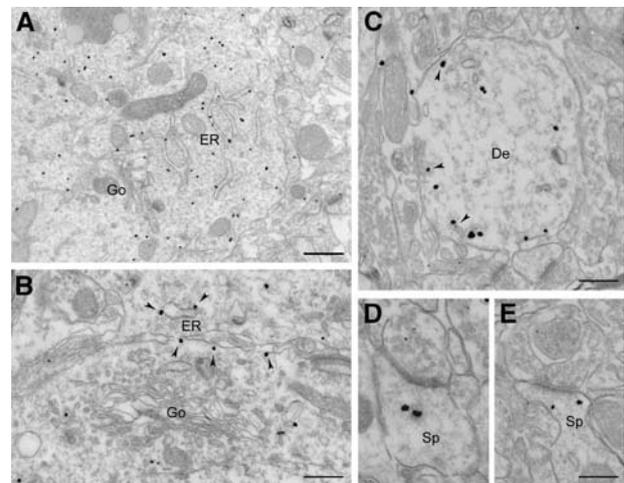
Figure 5 Electron micrographs showing immunogold labelling for CYP46A1 in the CA1 pyramidal neurons of the hippocampus. (**A**) CYP46A1 immunoreactivity is mainly associated with tubular structures belonging to the endoplasmic reticulum (ER) and is not present in the Golgi complex (Go). (**B**) Higher magnification image showing CYP46A1 immunoreactivity along ER tubules (arrowheads) but not in the Golgi. (**C**) CYP46A1 is present in the dendritic profiles, where it is often found in close proximity of the plasma membrane and tubular structures (arrowheads). (**D, E**) Localization of CYP46A1 in dendritic spines (Sp) receiving asymmetric synaptic contacts. Scale bars: (**A**) 800 nm; (**B, C**) 400 nm; (**D, E**) 200 nm.
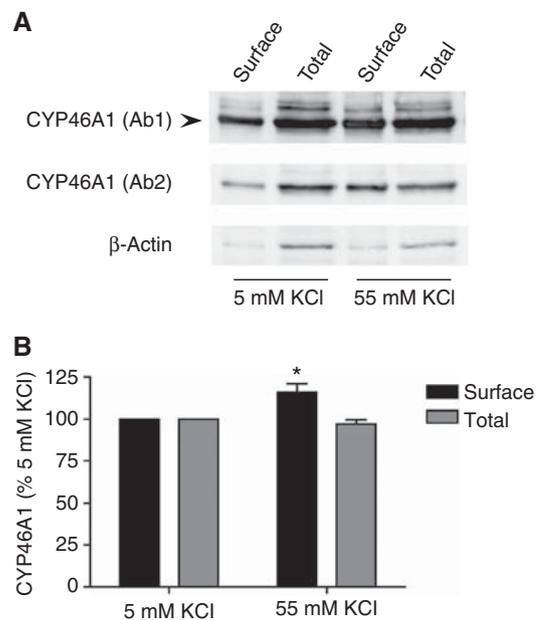
Figure 6 Excitatory neurotransmission induces CYP46A1 translocation to the plasma membrane. (**A**) Cultured hippocampal neurons were incubated with 5 or 55 mM buffer for 10 min, surface biotinylated with a membrane-impermeable biotin and lysed in STEN buffer. The lysates were incubated with streptavidin-coated sepharose beads, separated by SDS–PAGE and detected by immunoblotting using two different CYP46A1 antibodies (Ab 1: Russell's laboratory and Ab 2: ABCAM). Detection of β-actin was used as specificity control for surface labelling. (**B**) The amount of cell-surface CYP46A1 was normalized to the amount of total CYP46A1 in the cell lysate (input: 1/3 of the protein amount used in the pull-down), and the percentage of change was calculated. In steady-state conditions, $20.1 \pm 2.3\%$ of the total CYP46A1 pool was present at the surface. After stimulation with 55 mM KCl, neurons showed a significant increase in the amount of surface biotinylated CYP46A1, without changes in the total amount of protein ($n = 4$; *$P < 0.05$ versus 5 mM KCl, Student's *t*-test).
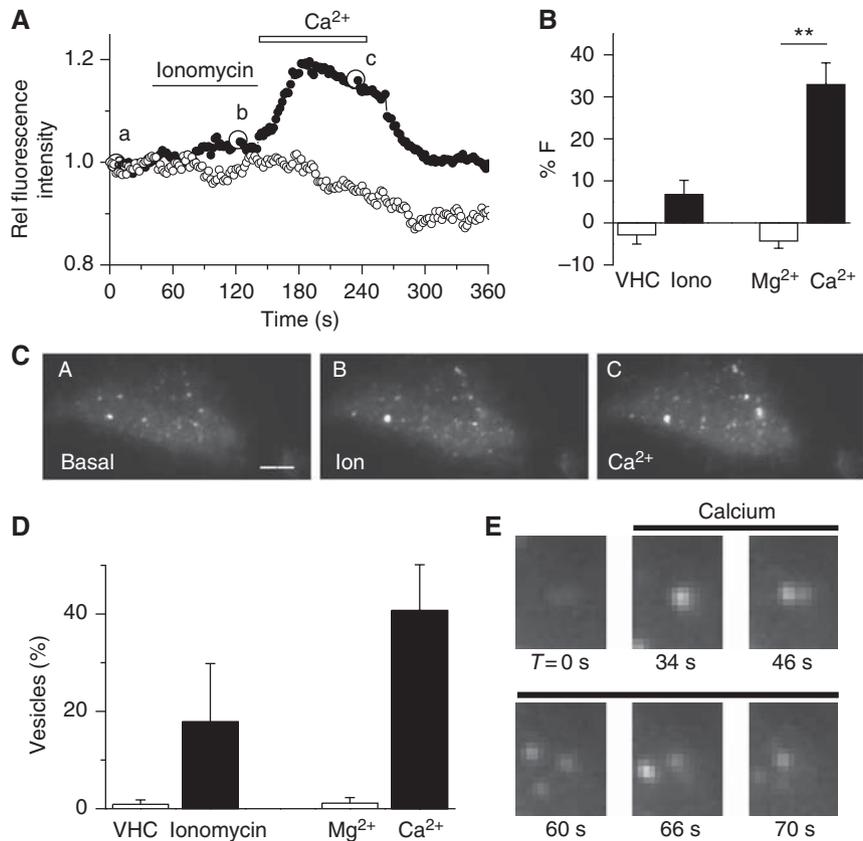
Figure 7 High intracellular Ca^{2+} mobilizes GFP–CYP46A1 towards the plasma membrane. (**A**) Relative change in the GFP–CYP46A1 fluorescence intensity as measured using Total Internal Reflection Microscopy (TIRF) after the addition of ionomycin and Ca^{2+} (black). For the negative controls (white), DMSO (vehicle) and Mg^{2+} were applied. (**B**) Average increase in fluorescence in the GFP–CYP46A1-expressing cells after different stimuli. (**C**) TIRF images of an HEK293T cell that expressed GFP–CYP46A1 at the time points indicated in (**A**) (a, before; b, after exposure to $0.5\,\mu M$ ionomycin; c, after addition of $2\,mM\ Ca^{2+}$). The scale bar indicates $4\,\mu m$. (**D**) Percentage of increase in the vesicle count following exposure to the indicated stimulus. (**E**) TIRF images of a GFP–CYP46A1-expressing HEK293T cell before ($t = 0$) and during external Ca^{2+} application ($**P < 0.002$, Student's t-test).

microscopy that allowed us to dynamically monitor GFP–CYP46A1 in the vicinity of the PM of transfected cells. Our first studies were performed in HEK cells, where the transfection efficiency is high. These cells were stimulated with $0.5\,\mu M$ ionomycin in the absence of extracellular Ca^{2+} to deplete the intracellular Ca^{2+} stores, and external Ca^{2+} was subsequently added to stimulate a store-dependent Ca^{2+} influx. Whereas stimulation with ionomycin caused only a modest increase in fluorescence ($9 \pm 3\%$, $n = 8$, $P = 0.06$), the subsequent addition of external Ca^{2+} induced a strong increase in the fluorescence intensity at and near the PM ($33 \pm 5\%$, $n = 8$, $P = 0.001$; Figure 7A and B; Supplementary Movie S1). The application of either vehicle or Mg^{2+}, instead of Ca^{2+}, did not cause any significant change in the amount of fluorescence ($n = 5$, Figure 7A and B). A detailed analysis of the TIRF images indicated that GFP–CYP46A1 was present in the punctae (vesicle-like structures). Consistent with the increase in total fluorescence, stimulation with ionomycin and Ca^{2+} increased the number of vesicle-like punctae that appeared in the evanescent field (19 ± 11 and $41 \pm 9\%$, respectively; Figure 7C and D). Moreover, during stimulation, we observed multiple punctae that rapidly increased their fluorescence and then abruptly disappeared, which we interpret as GFP–CYP46A1-containing vesicles that entered the evanescent field and subsequently fused with the PM

(Figure 7E). Similar TIRF studies performed in cultured hippocampal neurons stimulated with high K^+ confirmed these results (Figure 8; Supplementary Movies S2 and S3).

Discussion

We have shown that excitatory stimulation results in cholesterol loss in hippocampal neurons in culture, in purified synapses and in neurons *in vivo*. Because the major route of cholesterol removal is via CYP46A1 (Russell *et al*, 2009) and the main pool of cellular cholesterol is at the PM (Liscum and Munn, 1999; Pomorski *et al*, 2001), it is reasonable to propose that excitatory neurotransmission leads to cholesterol loss through the mobilization of CYP46A1 from its internal store, the ER, to the PM. The observed increase in surface CYP46A1 after stimulation supports this notion, and the higher production of the metabolite 24S-hydroxycholesterol in stimulated neurons prove that the pool of the enzyme that increase at the PM is active. Mechanistically, as one might have expected for an ER-resident protein, the process of cholesterol loss required high levels of intracellular Ca^{2+} and a functional STIM2. In fact, mice that were devoid of STIM2 (a Ca^{2+}-binding protein that is capable of sensing the ER Ca^{2+} levels (Brandman *et al*, 2007) that vary as a consequence of excitatory neurotransmission (Müller and Connor, 1991)) did not
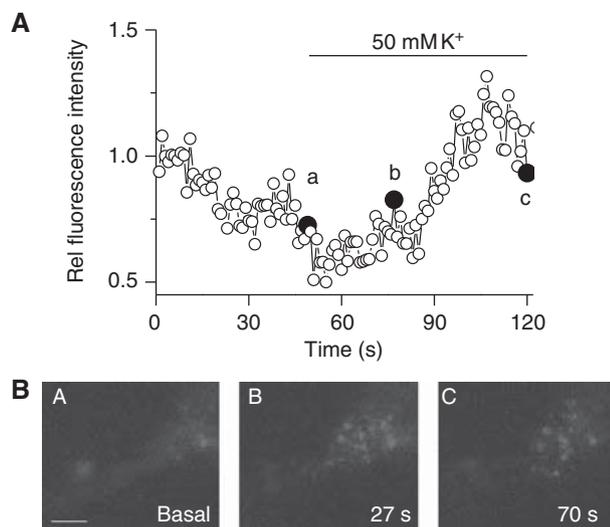
Figure 8 Neuronal stimulation mobilizes GFP–CYP46A1 towards the plasma membrane. (**A**) Time course of the normalized fluorescence intensity in the close vicinity of the plasma membrane measured by TIRF microscopy in 7 *div* hippocampal neurons transfected with GFP–CYP46, before and during stimulation with high K$^+$. (**B**) TIRF images at the time points indicated in (**A**). Scale bar: 10 µm.

show significant variations in synaptic cholesterol content upon the induction of glutamate release after an injection of KA.

It is known that the catalytic domain of CYP46A1 is in the C-terminus, facing the cytoplasmic side of the ER (Neve and Ingelman-Sundberg, 2010). Therefore, cholesterol loss that occurs after a rise in intracellular Ca^{2+} may be due to the proximity of this domain of the protein, still associated with the ER membrane, to cholesterol, in the cytoplasmic leaflet of the PM. However, our biotinylation experiments suggest that the C-terminus is exposed to the outer of the neurons (the N-terminus lacks lysines). This fact, together with the demonstration that the C-terminus faces the cytoplasmic side when the enzyme is in the ER membrane, raises the possibility that the ER, or an ER-derived carrier, interacts with the PM and allows CYP46A1 to flip and expose its catalytic domain to the outside of the cell, thus hydroxylating cholesterol from the outer leaflet. This model is consistent with another one that was proposed to explain the surface appearance of another member of the Cytochrome P450 family that increases on the outside of the hepatocyte's PM upon exposure to a drug that induces mobilization (Robin *et al*, 2000). Alternatively, cholesterol loss upon exposure to high levels of Ca^{2+} is the consequence of a dual mechanism: increased amounts of CYP46A1 at the PM (in the inner or the outer leaflet) and mobilization of cholesterol from the PM to the ER tubules to reach the cytoplasm-facing C-terminus of CYP46A1. Our TIRF results show vesicles entering the PM area; however, these results do not rule out the possibility that some of these vesicles are tethers of tubules that only approach the membrane, without true fusion. Irrespective of the precise mechanism through which cholesterol is lost, our results demonstrate the existence of an increase in the amount of plasma/juxta-PM CYP46A1 in conditions of high levels of intracellular Ca^{2+}. Because this enzyme is present in the ER and PM, but not in the Golgi, we favour the idea that

high levels of Ca^{2+} elicit a structural and functional communication between the SER and the PM, bypassing the Golgi apparatus. This process would be consistent with the observation that the distance between the ER and the PM can be as small as 10 nm (<30 nm is considered to be an association of the membranes) (Pichler *et al*, 2001; Wu *et al*, 2006; Lebiedzinska *et al*, 2009). In further agreement, it has been shown that NMDA receptor stimulation produces a transient and reversible fission of ER tubules (Kucharz *et al*, 2009).

In a similar manner to other biochemical changes that occur in conditions of excessive excitatory neurotransmission, one could postulate that the loss of cholesterol reported in this work is an exaggeration of physiological events that occur during steady-state excitation. However, the current lack of experimental tools capable of measuring small oscillations of the cholesterol content in spatially restricted areas (synapses) does not allow us to test this possibility. Hence, our results explain the early changes that occur on the PM during conditions characterized by a rapid increase in excitatory neurotransmission, such as epileptic seizures, brain trauma or stroke. In such scenarios, the cholesterol loss that is described in the present study will have a major impact on the physiology of the affected neurons. In fact, our results suggest that cholesterol loss modulates the intensity of intracellular calcium peaks in response to repetitive depolarization. Since cholesterol plays a key role in protein diffusion and endocytosis (Edidin, 2001; Lajoie and Nabi, 2007), this effect might be due to changes in the lateral diffusion and/or internalization rates of proteins involved in the control of the intracellular calcium concentration. In this scenario, we conclude that neurons that are exposed to a sudden rise in excitatory neurotransmission activate cholesterol loss mechanisms to protect themselves from death.

In the present study, we have shown that cholesterol loss is a normal response to high excitatory neurotransmission in neurons. This loss is due to increased intracellular Ca^{2+} and is paralleled by increased mobilization of the catabolic enzyme CYP46A1 from the smooth ER to the PM. Future work is required to establish whether or not manipulation of this phenomenon will prove therapeutically useful in the treatment of conditions characterized by abnormal excitatory neurotransmission, like epilepsy, brain trauma and stroke.

Materials and methods

Primary hippocampal cultures
Primary cultures were prepared using Wistar rat fetuses at embryonic day 18 (Kaech and Banker, 2006). For the biochemical analysis, dissociated cells were plated in 3 cm plastic dishes that were previously coated with 0.1 mg/ml of poly-L-lysine, at a density of 150 000 cells/dish. Neurons were grown for 14 days in minimal essential medium with N$_2$ supplement (MEM-N$_2$) at 37°C and under 5% CO$_2$.

Membrane purification from primary hippocampal cultures
Hippocampal neurons were scraped in 25 mM MES buffer (pH 7.0) that contained 2 mM EDTA and a protease inhibitor cocktail (Roche). Cells were lysed using a 22G needle and were spun at 0.5 g for 10 min to eliminate the nuclei. Then, the supernatant was centrifuged at 100 000 g for 1 h to obtain the membrane fraction. The membrane pellets were suspended in PBS (137 mM NaCl, 2.7 mM KCl, 10 mM Na$_2$HPO$_4$ and 1.76 mM KH$_2$PO$_4$; pH 7.4) that contained 0.2% SDS. The protein concentration of the samples was determined using the Bradford method (Bio-Rad Protein Microassay).

Mouse treatment with KA

Wild-type or STIM2 knockout mice were intraperitoneally injected with 20 mg/kg of KA (Sigma). After 30 min, the mice were sacrificed following the internal and European rules for animal care. The corresponding controls received intraperitoneal injections of a saline solution, which was the vehicle for the KA. Then, whole hippocampal membranes or synaptosomes were prepared for an analysis of their cholesterol levels.

Membrane purification from mouse hippocampi

After 30 min of treatment with saline or KA, hippocampi from C57BL/6J mice were dissected and homogenized in MES buffer using a glass-Teflon homogenizer and a 22G needle. Then, the homogenates were spun at $0.5\,g$ for 10 min to eliminate the nuclei, and the obtained supernatants were centrifuged at $100\,000\,g$ for 1 h to obtain the membrane fractions. The membrane pellets were suspended in PBS (137 mM NaCl, 2.7 mM KCl, 10 mM Na_2HPO_4 and 1.76 mM KH_2PO_4; pH 7.4) that contained 0.2% SDS. The protein concentration of the samples was determined using the Bradford method (Bio-Rad Protein Microassay).

Enzymatic cholesterol measurement

The cholesterol levels were assessed by fluorimetric detection using a commercial kit (Molecular Probes, Invitrogen). Briefly, cholesterol was oxidized using cholesterol oxidase to yield peroxide and the corresponding ketone. Peroxide was then detected using 10-acetyl-3,7-dihydroxyphenoxazine. This compound, in the presence of horseradish peroxidase, reacted with peroxide to produce highly fluorescent resorufin. Fluorescence was measured using a 1420 Multilabel Counter (VICTOR[3], Perkin-Elmer).

LC/MS lipid analysis

Lipids were extracted from brain tissue and cultured neurons according to the method of Bligh and Dyer (1959). Lipid phosphorus content of the extract was measured according to the method of Rouser *et al* (1970). Phospholipid content of cultured neurons was determined by LC/MS, using authentic standards as external calibrators. For medium analysis, 5 ml of the medium was applied to solid phase extraction columns (500 mg Lichrolute RP18, obtained from Merck, Darmstadt, Germany) that were previously activated by washing with 4 ml of methanol and water, respectively. After subsequent washing with 3 ml of water, hydrophobic compounds were eluted with 1 ml of methanol and 2 ml of chloroform/methanol (1:2, v/v). The combined organic phase was evaporated under nitrogen and samples were stored at $-20^\circ C$ under nitrogen atmosphere until analysed. Sterols (including cholesterol and 24S-hydroxycholesterol) were analysed as previously described, using 4-cholesten-3-on as an internal standard (Brouwers *et al*, 2011).

Surface biotinylation

Biotinylation of PM CYP46A1 was performed using a membrane-impermeable biotin. Hippocampal cultures were washed with ice-cold PBS and were incubated with 50 μg/ml of EZ-link Sulfo-NHS-Biotin (Pierce) for 30 min at 4°C. Any excess biotin was quenched by washing the cultures three times with 20 mM glycine. Then, the cells were lysed in an STEN-lysis buffer (50 mM TRIS, 150 mM NaCl, 2 mM EDTA, 1% Triton X-100 and 1% NP-40; pH 7.6), and the biotinylated proteins that were present in the lysate were pulled down using streptavidin-sepharose beads (GE Healthcare). The cell-surface CYP46A1 was detected using western immunoblotting, and the quantifications were performed using ImageJ 1.37v software (NIH, USA). The signal of the streptavidin pull-down (surface CYP46A1) was normalized by the input (total CYP46A1), and the percentage of change was calculated.

Purification and stimulation of synaptosomes

Synaptosomes were prepared from adult Wistar rats or C57BL/6J mice, as previously described (Pilo Boyl *et al*, 2007; Napoli *et al*, 2008). Briefly, the brains were quickly removed, the olfactory bulb and cerebellum were dissected, and both hemispheres were put into an ice-cold buffer solution (320 mM sucrose, 1 mM EDTA and 5 mM HEPES; pH 7.4). After homogenization with eight strokes in a glass-Teflon homogenizer, the homogenate was centrifuged at $3000\,g$ for 10 min. Then, the supernatant was centrifuged at $14\,000\,g$ for 10 min. The pelleted synaptosomes were resuspended in Kreb's-Ringer buffer (140 mM NaCl, 5 mM KCl, 5 mM glucose, 1 mM EDTA

and 10 mM HEPES; pH 7.4) and were mixed with Percoll to reach a final Percoll concentration of 45%. The samples were centrifuged at $18\,000\,g$ for 2 min, and the enriched synaptosomes were recovered from the top of the solution and were washed by spinning them for 30 s at $18\,000\,g$. The pelleted, enriched synaptosomes were resuspended in HEPES buffer (140 mM NaCl, 5 mM KCl, 10 mM glucose, 2 mM $MgSO_4$, 2 mM $CaCl_2$ and 20 mM HEPES; pH 7.4). After 30 min of stabilization at 37°C, the synaptosomal fractions were treated with different drugs or were incubated in a depolarizing buffer (90 mM NaCl, 55 mM KCl, 10 mM glucose, 2 mM $MgSO_4$, 2 mM $CaCl_2$ and 20 mM HEPES; pH 7.4). The experiments were completed by placing the samples on ice. Then, synaptosomal membranes were obtained by centrifugation at $100\,000\,g$ for 1 h. The membrane pellets were resuspended in PBS with 0.2% SDS. Then, the protein content was measured using the Bradford method (Bio-Rad Protein Microassay), and the cholesterol levels were assessed using fluorimetric detection (Molecular Probes, Invitrogen).

For the evaluation of calcium dependency, the following buffers were used: 5 mM KCl buffer (130 mM NaCl, 5 mM KCl, 2.2 mM $CaCl_2$, 4 mM $NaHCO_3$, 5.6 mM glucose, 0.5 mM Na_2HPO_4, 0.4 mM KH_2PO_4 and 10 mM HEPES, pH 7.4); 55 mM KCl buffer (80 mM NaCl, 55 mM KCl, 2.2 mM $CaCl_2$, 4 mM $NaHCO_3$, 5.6 mM glucose, 0.5 mM Na_2HPO_4, 0.4 mM KH_2PO_4 and 10 mM HEPES, pH 7.4); 5 mM KCl buffer/EGTA (130 mM NaCl, 5 mM KCl, 1 mM EGTA, 4 mM $NaHCO_3$, 5.6 mM glucose, 0.5 mM Na_2HPO_4, 0.4 mM KH_2PO_4 and 10 mM HEPES, pH 7.4); and 55 mM KCl buffer/EGTA (80 mM NaCl, 55 mM KCl, 1 mM EGTA, 4 mM $NaHCO_3$, 5.6 mM glucose, 0.5 mM Na_2HPO_4, 0.4 mM KH_2PO_4 and 10 mM HEPES, pH 7.4).

STIM2 knockouts

The generation of $Stim2^{-/-}$ mice has been recently reported (Berna-Erro *et al*, 2009). The mice used in the experiments were at least 3 months of age. All of the animal manipulations were approved by the local authorities and were conducted according to the German law of animal protection.

Calcium imaging

Changes in intracellular calcium concentration in rat hippocampal neurons were monitored using ratiometric Fura-2-based fluorimetry. Hippocampal neurons plated on glass coverslips were loaded with 5 μM Fura-2AM-ester (Alexis Biochemicals) for 30 min. Fluorescence was measured during repetitive illumination at 340 and 380 nm with a monochromator-based imaging system. The ratio of the fluorescence signal at both wavelengths was calculated as previously described (Vriens *et al*, 2005). The standard extracellular solution contained (in mM): 138 NaCl, 5.4 KCl, 2 $CaCl_2$, 2 $MgCl_2$, 10 glucose and 10 HEPES (pH 7.4). The high K^+ solution for stimulation contained (in mM): 95 NaCl, 50 KCl, 2 $CaCl_2$, 2 $MgCl_2$, 10 glucose and 10 HEPES (pH 7.4). Experiments were performed at room temperature.

The Krebs solution applied in between the two high potassium stimuli in order to deliver small amounts of cholesterol contained a combination of 30 μM Sigma water-soluble cholesterol and 5.2 μM cholesterol (plus 10 μM NMDA). To remove small amounts of membrane cholesterol, 0.1 mM MBCD was added in the Krebs solution.

Electron microscopy

Adult mice were anaesthetized using an intraperitoneal injection of xylazine (0.25 mg; Rompun; Bayer Health Care) and ketamine (2.5 mg; Imalgene; Merial). The mice were then perfused with 2% formaldehyde and 0.05% glutaraldehyde in a sodium acetate buffer (0.1 M, pH 6.0) for 2 min, followed by a 1 h perfusion with 2% formaldehyde and 0.05% glutaraldehyde in a borate buffer (0.1 M, pH 9.0). The brain was dissected, post-fixed overnight, and then sliced into 80 μm coronal sections through the dorsal hippocampus using a vibratome (Leica VT 1000S). These sections were cryoprotected in 30% sucrose and were then frozen and thawed three times to enhance the antibody penetration. The sections were then collected in PBS, blocked in 10% normal goat serum (NGS) and incubated with a polyclonal antibody against CYP46A1 (1:400 in TBS) at 4°C for 72 h. The sections were then incubated with secondary antibodies that were coupled to 1.4 nm colloidal gold particles (1:100; Alexa Fluor-488 FluoNanogold anti-rabbit Fab; Nanoprobes Inc., Yaphank, NY). Ultrasmall gold particles were visualized with the gold enhance EM formulation (Nanoprobes), as

described by the manufacturer. Lastly, the sections were post-fixed with 0.5% osmium tetroxide for 15 min at 4°C, stained with 1% uranyl acetate for 25 min, dehydrated in acetone and flat-embedded in Epon 812. Ultrathin sections were collected on 400 mesh copper grids, stained with lead citrate for 3 min and observed with a JEM-1010 electron microscope (Jeol, Japan) that was equipped with a side-mounted CCD camera (Mega View III; Soft Imaging System, Germany).

TIRF microscopy

Human embryonic kidney cells, HEK293T, were grown in Dulbecco's modified Eagle's medium (DMEM) that contained 10% (v/v) human serum, 2 mM L-glutamine, 2 units/ml penicillin and 2 mg/ml streptomycin at 37°C in a humidity-controlled incubator with 10% CO_2. HEK293T cells were transiently transfected with cDNA encoding GFP–CYP46A1 using the TransIT-Neural Transfection Reagent (Mirus Corporation, Madison, USA). The GFP–CYP46A1 (with GFP in the C-terminus) was produced in our laboratory. The mouse *CYP46A1* gene was amplified from the expression vector pT-Rex-DEST30 (RZPD, Berlin, Germany) using the following primers: 5′-GCCACCATGAGCCCCGGGCTGCTGCTG-3′ and 3′-GGATCCGAGCAGGGTGGGGGTGGGGGTGC-5′. Then, the cDNA was subcloned into the pEGFP-N1 plasmid (Clontech Laboratories, Inc) using the ApaI and BamHI restriction sites.

All of the live-imaging experiments were performed at 25°C with cells that were grown on 25 mm glass coverslips and were placed in a custom chamber with HEPES-buffered saline that contained (in mM): 150 NaCl, 5 $MgCl_2$, 1 EGTA, 10 HEPES (pH 7.4). When indicated, the EGTA was replaced by 3 mM $CaCl_2$. Cells were imaged 3 days after transfection. TIRF images (150 ms exposure) were acquired using a through-the-lens TIRF system that was built around an inverted Axio Observer.Z1 microscope equipped with a X-100 oil objective (numerical aperture = 1.45) and a Hamamatsu Orca-R^2 camera. We excited the GFP–CYP46A1 using a 488-nm laser, and excitation and emission light was separated using appropriate filters. Time series of 250 images at 2 s intervals were recorded. Constant laser intensity, focus (Definite Focus Zeiss), TIRF angle and camera gain were maintained throughout each experiment. The spatially averaged fluorescence intensity (i.e., averaged over the entire region of the cell being imaged) was determined using Axiovision 4.8. Images were analysed using a laboratory-developed software to determine the amount of vesicles in each image. This program discriminates between moving vesicles and the background by subtracting from each frame an average image that was calculated from a user-selectable number of frames surrounding the frame of interest. The user then provides an intensity level value (0–255), which is used to convert the 8-bit grayscale image that is obtained using background cancellation to a monochrome image that contains only the isolated particles. This frame is fed to a particle analysis routine that detects and counts the number of vesicles, analyses the particle shape and provides the output as a human-readable ASCII file. The software was created using the NI LabWindows™/CVI development package and image processing libraries from the NI Vision Development Module, both of which were obtained from National Instruments Belgium (NV/SA, 1930 Zaventem, Belgium).

Hippocampal neurons were transfected with cDNA encoding GFP–CYP46A1 using the TransIT-Neural Transfection Reagent (Mirus Corporation), following manufacturer's protocol.

shRNA and lentivirus preparation

The CYP46A1 targeting sequence was designed using the RNAi design algorithm at http://www.dharmacon.com/DesignCenter/DesignCenterPage.aspx. Then, 46-sense and 46-antisense oligos encoding CYP46A1-shRNA were designed as previously reported (Rubinson *et al*, 2003). The pSi46 plasmid was constructed by cloning the 46-sense/antisense duplexes into the pLentiLox 3.7 and lentiviral particles were produced as previously described (Martin *et al*, 2008).

Statistical analysis

Protein normalized cholesterol levels in cultured hippocampal neurons and synaptosomes (Figures 1A and 2A) were compared with those of the corresponding controls for each treatment using Student's *t*-test. Then, the percentage of change compared with the corresponding controls was calculated for each treatment, and all of the variations were plotted in the same graph, with a unique representative bar for the controls (100%). In the remainder of the experiments, Student's *t*-test was applied as stated in the figure legends. Differences between groups were considered to be significant when $P < 0.05$.

Supplementary data

Supplementary data are available at *The EMBO Journal* Online (http://www.embojournal.org).

Conflict of interest

The authors declare that they have no conflict of interest.

References

Ben-Ari Y, Cossart R (2000) Kainate, a double agent that generates seizures: two decades of progress. *Trends Neurosci* **23:** 580–587

Berna-Erro A, Braun A, Kraft R, Kleinschnitz C, Schuhmann MK, Stegner D, Wultsch T, Eilers J, Meuth SG, Stoll G, Nieswandt B (2009) STIM2 regulates capacitive Ca2 + entry in neurons and plays a key role in hypoxic neuronal cell death. *Sci Signal* **2:** ra67

Björkhem I, Meaney S (2004) Brain cholesterol: long secret life behind a barrier. *Arterioscler Thromb Vasc Biol* **24:** 806–815

Bligh EG, Dyer WJ (1959) A rapid method of total lipid extraction and purification. *Can J Biochem Physiol* **37:** 911–917

Brandman O, Liou J, Park WS, Meyer T (2007) STIM2 is a feedback regulator that stabilizes basal cytosolic and endoplasmic Ca2 + levels. *Cell* **131:** 1327–1339

Brouwers JF, Boerke A, Silva PFN, Garcia-Gil N, van Gestel RA, Helms JB, van de Lest CHA, Gadella BM (2011) Mass spectrometric detection of cholesterol oxidation in bovine sperm. *Biol Reprod* **85:** 128–136

Dietschy JM, Turley SD (2004) Thematic review series: brain lipids. Cholesterol metabolism in the central nervous system during early development and in the mature animal. *J Lipid Res* **45:** 1375–1397

Edidin M (2001) Shrinking patches and slippery rafts: scales of domains in the plasma membrane. *Trends Cell Biol* **11:** 492–496

Frank C, Rufini S, Tancredi V, Forcina R, Grossi D, D'Arcangelo G (2008) Cholesterol depletion inhibits synaptic transmission and synaptic plasticity in rat hippocampus. *Exp Neurol* **212:** 407–414

Gong JS, Kobayashi M, Hayashi H, Zou K, Sawamura N, Fujita SC, Yanagisawa K, Michikawa M (2002) Apolipoprotein E (ApoE) isoform-dependent lipid release from astrocytes prepared from human ApoE3 and ApoE4 knock-in mice. *J Biol Chem* **277:** 29919–29926

Göritz C, Mauch DH, Nägler K, Pfrieger FW (2002) Role of glia-derived cholesterol in synaptogenesis: new revelations in the synapse-glia affair. *J Physiol Paris* **96:** 257–263

Jahn R, Südhof TC (1994) Synaptic vesicles and exocytosis. *Annu Rev Neurosci* **17:** 219–246

Kaech S, Banker G (2006) Culturing hippocampal neurons. *Nat Protoc* **1:** 2406–2415

Kucharz K, Krogh M, Ng AN, Toresson H (2009) NMDA receptor stimulation induces reversible fission of the neuronal endoplasmic reticulum. *PLoS One* **4:** e5250

Lajoie P, Nabi IR (2007) Regulation of raft-dependent endocytosis. *J Cell Mol Med* **11:** 644–653

Lange Y (1991) Disposition of intracellular cholesterol in human fibroblasts. *J Lipid Res* **32:** 329–339

Lebiedzinska M, Szabadkai G, Jones AW, Duszynski J, Wieckowski MR (2009) Interactions between the endoplasmic reticulum, mitochondria, plasma membrane and other subcellular organelles. *Int J Biochem Cell Biol* **41:** 1805–1816

Léveillé F, Papadia S, Fricker M, Bell KF, Soriano FX, Martel MA, Puddifoot C, Habel M, Wyllie DJ, Ikonomidou C, Tolkovsky AM, Hardingham GE (2010) Suppression of the intrinsic apoptosis pathway by synaptic activity. *J Neurosci* **30:** 2623–2635

Lingwood D, Simons K (2010) Lipid rafts as a membrane-organizing principle. *Science* **327:** 46–50

Liscum L, Munn NJ (1999) Intracellular cholesterol transport. *Biochim Biophys Acta* **1438:** 19–37

Liu SJ, Zukin RS (2007) Ca2 +-permeable AMPA receptors in synaptic plasticity and neuronal death. *Trends Neurosci* **30:** 126–134

Lund EG, Guileyardo JM, Russell DW (1999) cDNA cloning of cholesterol 24-hydroxylase, a mediator of cholesterol homeostasis in the brain. *Proc Natl Acad Sci USA* **96:** 7238–7243

Lütjohann D (2006) Cholesterol metabolism in the brain: importance of 24S-hydroxylation. *Acta Neurol Scand* **114:** 33–42

Mans RA, Chowdhury N, Cao D, McMahon LL, Li L (2010) Simvastatin enhances hippocampal long-term potentiation in C57BL/6 mice. *Neuroscience* **166:** 435–448

Martin MG, Perga S, Trovò L, Rasola A, Holm P, Rantamäki T, Harkany T, Castrén E, Chiara F, Dotti CG (2008) Cholesterol loss enhances TrkB signaling in hippocampal neurons aging *in vitro*. *Mol Biol Cell* **19:** 2101–2112

Michikawa M, Fan QW, Isobe I, Yanagisawa K (2000) Apolipoprotein E exhibits isoform-specific promotion of lipid efflux from astrocytes and neurons in culture. *J Neurochem* **74:** 1008–1016

Müller W, Connor JA (1991) Dendritic spines as individual neuronal compartments for synaptic Ca2 + responses. *Nature* **354:** 73–76

Napoli I, Mercaldo V, Boyl PP, Eleuteri B, Zalfa F, De Rubeis S, Di Marino D, Mohr E, Massimi M, Falconi M, Witke W, Costa-Mattioli M, Sonenberg N, Achsel T, Bagni C (2008) The fragile X syndrome protein represses activity-dependent translation through CYFIP1, a new 4E-BP. *Cell* **134:** 1042–1054

Neve EP, Ingelman-Sundberg M (2010) Cytochrome P450 proteins: retention and distribution from the endoplasmic reticulum. *Curr Opin Drug Discov Devel* **13:** 78–85

Nicholls DG, Chalmers S (2004) The integration of mitochondrial calcium transport and storage. *J Bioenerg Biomembr* **36:** 277–281

Nieweg K, Schaller H, Pfrieger FW (2009) Marked differences in cholesterol synthesis between neurons and glial cells from postnatal rats. *J Neurochem* **109:** 125–134

Ong WY, Kim JH, He X, Chen P, Farooqui AA, Jenner AM (2010) Changes in brain cholesterol metabolome after excitotoxicity. *Mol Neurobiol* **41:** 299–313

Papadia S, Hardingham GE (2007) The dichotomy of NMDA receptor signalling. *Neuroscientist* **13:** 572–579

Papadia S, Soriano FX, Léveillé F, Martel MA, Dakin KA, Hansen HH, Kaindl A, Sifringer M, Fowler J, Stefovska V, McKenzie G, Craigon M, Corriveau R, Ghazal P, Horsburgh K, Yankner BA, Wyllie DJ, Ikonomidou C, Hardingham GE (2008) Synaptic NMDA receptor activity boosts intrinsic antioxidant defenses. *Nat Neurosci* **11:** 476–487

Pichler H, Gaigg B, Hrastnik C, Achleitner G, Kohlwein SD, Zellnig G, Perktold A, Daum G (2001) A subfraction of the yeast endoplasmic reticulum associates with the plasma membrane and has a high capacity to synthesize lipids. *Eur J Biochem* **268:** 2351–2361

Pilo BP, Di Nardo A, Mulle C, Sassoè-Pognetto M, Panzanelli P, Mele A, Kneussel M, Costantini V, Perlas E, Massimi M, Vara H, Giustetto M, Witke W (2007) Profilin2 contributes to synaptic vesicle exocytosis, neuronal excitability, and novelty-seeking behavior. *EMBO J* **26:** 2991–3002

Pomorski T, Hrafnsdóttir S, Devaux PF, van Meer G (2001) Lipid distribution and transport across cellular membranes. *Semin Cell Dev Biol* **12:** 139–148

Ramirez DMO, Anderson S, Russell DW (2008) Neuronal expression and subcellular localization of cholesterol 24-hydroxylase in the mouse brain. *J Comp Neurol* **507:** 1676–1693

Renner M, Choquet D, Triller A (2009) Control of the postsynaptic membrane viscosity. *J Neurosci* **29:** 2926–2937

Robin MA, Descatoire V, Le Roy M, Berson A, Lebreton FP, Maratrat M, Ballet F, Loeper J, Pessayre D (2000) Vesicular transport of newly synthesized cytochromes P4501A to the outside of rat hepatocyte plasma membranes. *J Pharmacol Exp Ther* **294:** 1063–1069

Rodal SK, Skretting G, Garred O, Vilhardt F, van Deurs B, Sandvig K (1999) Extraction of cholesterol with methyl-beta-cyclodextrin perturbs formation of clathrin-coated endocytic vesicles. *Mol Biol Cell* **10:** 961–974

Rogers TB, Inesi G, Wade R, Lederer WJ (1995) Use of thapsigargin to study Ca2 + homeostasis in cardiac cells. *Biosci Rep* **15:** 341–349

Rouser G, Fkeischer S, Yamamoto A (1970) Two dimensional thin layer chromatographic separation of polar lipids and determination of phospholipids by phosphorus analysis of spots. *Lipids* **5:** 494–496

Rubinson DA, Dillon CP, Kwiatkowski AV, Sievers C, Yang L, Kopinja J, Rooney DL, Zhang M, Ihrig MM, McManus MT, Gertler FB, Scott ML, Van Parijs L (2003) A lentivirus-based system to functionally silence genes in primary mammalian cells, stem cells and transgenic mice by RNA interference. *Nat Genet* **33:** 401–406

Ruiz A, Matute C, Alberdi E (2009) Endoplasmic reticulum Ca(2 +) release through ryanodine and IP(3) receptors contributes to neuronal excitotoxicity. *Cell Calcium* **46:** 273–281

Russell DW, Halford RW, Ramirez DMO, Shah R, Kotti T (2009) Cholesterol 24-hydroxylase: an enzyme of cholesterol turnover in the brain. *Annu Rev Biochem* **78:** 1017–1040

Schubert V, Da Silva JS, Dotti CG (2006) Localized recruitment and activation of RhoA underlies dendritic spine morphology in a glutamate receptor-dependent manner. *J Cell Biol* **172:** 453–467

Simons K, Toomre D (2000) Lipid rafts and signal transduction. *Nat Rev Mol Cell Biol* **1:** 31–39

Szczesna-Skorupa E, Ahn K, Chen CD, Doray B, Kemper B (1995) The cytoplasmic and N-terminal transmembrane domains of cytochrome P450 contain independent signals for retention in the endoplasmic reticulum. *J Biol Chem* **270:** 24327–24333

Tarasenko AS, Sivko RV, Krisanova NV, Himmelreich NH, Borisova TA (2010) Cholesterol depletion from the plasma membrane impairs proton and glutamate storage in synaptic vesicles of nerve terminals. *J Mol Neurosci* **41:** 358–367

Tsui-Pierchala BA, Encinas M, Milbrandt Jr J, Johnson EM (2002) Lipid rafts in neuronal signaling and function. *Trends Neurosci* **25:** 412–417

Verkhratsky A (2002) The endoplasmic reticulum and neuronal calcium signalling. *Cell Calcium* **32:** 393–404

Vriens J, Owsianik G, Fisslthaler B, Suzuki M, Janssens A, Voets T, Morisseau C, Hammock BD, Fleming I, Busse R, Nilius B (2005) Modulation of the Ca2 permeable cation channel TRPV4 by cytochrome P450 epoxygenases in vascular endothelium. *Circ Res* **97:** 908–915

Wu MM, Buchanan J, Luik RM, Lewis RS (2006) Ca2 + store depletion causes STIM1 to accumulate in ER regions closely associated with the plasma membrane. *J Cell Biol* **174:** 803–813

Yuste R, Majewska A, Holthoff K (2000) From form to function: calcium compartmentalization in dendritic spines. *Nat Neurosci* **3:** 653–659